Conceptual design of the AGATA 1π array at GANIL

E. Clément, C. Michelagnoli, G. De France, H.J. Li, A. Lemasson, M. Beuzard, C. Barthe Dejean, P. Bougault, J. Cacitti, J.-L. Foucher, et al.

▶ **To cite this version:**

E. Clément, C. Michelagnoli, G. De France, H.J. Li, A. Lemasson, et al.. Conceptual design of the AGATA 1π array at GANIL. Nuclear Instruments and Methods in Physics Research Section A: Accelerators, Spectrometers, Detectors and Associated Equipment, 2017, 855, pp.1-12. 10.1016/j.nima.2017.02.063 . cea-01538475

HAL Id: cea-01538475
https://cea.hal.science/cea-01538475v1

Submitted on 7 Feb 2022

HAL is a multi-disciplinary open access archive for the deposit and dissemination of scientific research documents, whether they are published or not. The documents may come from teaching and research institutions in France or abroad, or from public or private research centers.

L'archive ouverte pluridisciplinaire **HAL**, est destinée au dépôt et à la diffusion de documents scientifiques de niveau recherche, publiés ou non, émanant des établissements d'enseignement et de recherche français ou étrangers, des laboratoires publics ou privés.

Nuclear Instruments and Methods in Physics Research A 855 (2017) 1–12

Contents lists available at ScienceDirect

Nuclear Instruments and Methods in Physics Research A

journal homepage: www.elsevier.com/locate/nima

Conceptual design of the AGATA 1π array at GANIL

E. Clément[a,*], C. Michelagnoli[a], G. de France[a], H.J. Li[a], A. Lemasson[a], C. Barthe Dejean[a], M. Beuzard[a], P. Bougault[a], J. Cacitti[a], J.-L. Foucher[a], G. Fremont[a], P. Gangnant[a], J. Goupil[a], C. Houarner[a], M. Jean[a], A. Lefevre[a], L. Legeard[a], F. Legruel[a], C. Maugeais[a], L. Ménager[a], N. Ménard[a], H. Munoz[a], M. Ozille[a], B. Raine[a], J.A. Ropert[a], F. Saillant[a], C. Spitaels[a], M. Tripon[a], Ph. Vallerand[a], G. Voltolini[a], W. Korten[b], M.-D. Salsac[b], Ch. Theisen[b], M. Zielińska[b], T. Joannem[b], M. Karolak[b], M. Kebbiri[b], A. Lotode[b], R. Touzery[b], Ch. Walter[b], A. Korichi[c], J. Ljungvall[c], A. Lopez-Martens[c], D. Ralet[c], N. Dosme[c], X. Grave[c], N. Karkour[c], X. Lafay[c], E. Legay[c], I. Kojouharov[d], C. Domingo-Pardo[e], A. Gadea[e], R.M. Pérez-Vidal[e], J.V. Civera[e], B. Birkenbach[f], J. Eberth[f], H. Hess[f], L. Lewandowski[f], P. Reiter[f], A. Nannini[g], G. De Angelis[h], G. Jaworski[h], P. John[h], D.R. Napoli[h], J.J. Valiente-Dobón[h], D. Barrientos[h], D. Bortolato[h], G. Benzoni[i], A. Bracco[i], S. Brambilla[i], F. Camera[i], F.C.L. Crespi[i], S. Leoni[i], B. Million[i], A. Pullia[i], O. Wieland[i], D. Bazzacco[j], S.M. Lenzi[j], S. Lunardi[j], R. Menegazzo[j], D. Mengoni[j], F. Recchia[j], M. Bellato[j], R. Isocrate[j], F.J. Egea Canet[j], F. Didierjean[k], G. Duchêne[k], R. Baumann[k], M. Brucker[k], E. Dangelser[k], M. Filliger[k], H. Friedmann[k], G. Gaudiot[k], J.-N. Grapton[k], H. Kocher[k], C. Mathieu[k], M.-H. Sigward[k], D. Thomas[k], S. Veeramootoo[k], J. Dudouet[l], O. Stézowski[l], C. Aufranc[l], Y. Aubert[m], M. Labiche[n], J. Simpson[n], I. Burrows[n], P.J. Coleman-Smith[n], A. Grant[n], I.H. Lazarus[n], P.S. Morrall[n], V.F.E. Pucknell[n], A. Boston[o], D.S. Judson[o], N. Lalović[p,q], J. Nyberg[r], J. Collado[s], V. González[s], I. Kuti[t], B.M. Nyakó[t], A. Maj[u], M. Rudigier[v]

[a] Grand Accélérateur National d'Ions Lourds (GANIL), CEA/DRF-CNRS/IN2P3, F-14076 Caen Cedex 05, France
[b] Irfu, CEA, Université Paris-Saclay, 91191 Gif-sur-Yvette, France
[c] CSNSM, Université Paris-Sud, CNRS/IN2P3, Université Paris-Saclay, 91405 Orsay, France
[d] GSI Helmholtzzentrum für Schwerionenforschung mbH, Darmstadt, Germany
[e] Instituto de Física Corpuscular, CSIC - Universidad de Valencia, E-46980 Paterna, Valencia, Spain
[f] IKP, University of Cologne, D-50937 Cologne, Germany
[g] INFN Sezione di Firenze, IT-50019 Sesto Fiorentino, Italy
[h] INFN Laboratori Nazionali di Legnaro, IT-35020 Legnaro, Italy
[i] INFN Sezione di Milano, IT-20133 Milano, Italy
[j] INFN Sezione di Padova and Dipartimento di Fisica e Astronomia dell'Universita', I-35131 Padova, Italy
[k] Université de Strasbourg, CNRS, IPHC, UMR 7178, F-67000 Strasbourg, France
[l] Institut de Physique Nucléaire de Lyon, Université de Lyon, Université Lyon 1, CNRS-IN2P3, F-69622 Villeurbanne, France
[m] Institut de Physique Nucléaire d'Orsay, Université Paris-Sud, CNRS/IN2P3, Université Paris-Saclay, 91405 Orsay, France
[n] STFC Daresbury Laboratory, Daresbury, Warrington WA4 4AD, United Kingdom
[o] Oliver Lodge Laboratory, The University of Liverpool, Oxford Street, Liverpool L69 7ZE, United Kingdom
[p] Department of Physics, Lund University, Lund, Sweden
[q] GSI Helmholtzzentrum für Schwerionenforschung mbH, Darmstadt, Germany
[r] Department of Physics and Astronomy, Uppsala University, Uppsala, Sweden
[s] Department of Electronic Engineering, University of Valencia, E-46100 Burjassot, Valencia, Spain
[t] Institute for Nuclear Research, Hungarian Academy of Sciences, Pf. 51, 4001 Debrecen, Hungary
[u] Institute of Nuclear Physics, Polish Academy of Sciences, PL 31-342 Kraków, Poland
[v] Department of Physics, University of Surrey, Guildford, United Kingdom

ARTICLE INFO

Keywords:
AGATA spectrometer

ABSTRACT

The Advanced GAmma Tracking Array (AGATA) has been installed at the GANIL facility, Caen-France. This set-up exploits the stable and radioactive heavy-ions beams delivered by the cyclotron accelerator complex of

* Corresponding author.

http://dx.doi.org/10.1016/j.nima.2017.02.063
Received 9 January 2017; Received in revised form 16 February 2017; Accepted 20 February 2017
Available online 24 February 2017
0168-9002/ © 2017 Elsevier B.V. All rights reserved.

GANIL facility
γ-ray tracking
Pulse shape analysis
VAMOS++ spectrometer
NEDA detector
DIAMANT detector
PARIS $LaBr_3$ detector
FATIMA $LaBr_3$ detector
Plunger device

GANIL. Additionally, it benefits from a large palette of ancillary detectors and spectrometers to address in-beam γ-ray spectroscopy of exotic nuclei. The set-up has been designed to couple AGATA with a magnetic spectrometer, charged-particle and neutron detectors, scintillators for the detection of high-energy γ rays and other devices such as a plunger to measure nuclear lifetimes. In this paper, the design and the mechanical characteristics of the set-up are described. Based on simulations, expected performances of the AGATA 1π array are presented.

1. Introduction

High-resolution γ-ray spectroscopy plays a major role in nuclear structure, nuclear astrophysics and nuclear-reaction mechanism studies. Continuous progress in detector technology and data analysis leads to improved sensitivity giving access to more exotic nuclei and detailed nuclear spectroscopic information such as transition rates or electromagnetic moments. In recent years, dedicated set-ups coupling large high-purity Ge arrays with ancillary detectors, such as magnetic spectrometers or separators, scintillators for high energy γ-ray detection or fast-timing measurements, or particle detectors, have been developed in large scale heavy-ion facilities. Thanks to these improvements, high resolution γ-ray spectroscopy of exotic nuclei was performed with unprecedented sensitivity over the nuclear chart, from light to heavy nuclei, and from the proton to the neutron drip-lines.

Moderately neutron-rich as well as proton-rich exotic nuclei can be populated by multi-nucleon transfer or deep-inelastic collision [1,2]. The use of a magnetic spectrometer, such as the S800 spectrograph [3], the PRISMA [4] or the VAMOS++ spectrometers [5], placed at an angle covering the grazing angle of the reaction, coupled to large γ-arrays, such as the SeGA [6], the GRETINA [7,8], the CLARA [9] or the EXOGAM [10] arrays, allows in-beam γ-ray spectroscopy of these exotic nuclei. More specifically, at GANIL, the use of heavy ion beams such as Pb or U elements brings a significant gain in sensitivity in the laboratory frame thanks to the inverse kinematic. Another efficient reaction mechanism for the production of neutron-rich nuclei is fusion-fission using heavy ion beams and light targets in which the fission fragments are identified with the spectrometer placed at the folding angle of the fission cone [11]. Prompt γ-ray spectroscopy of very neutron-deficient isotopes is performed at stable ion beam facilities using fusion-evaporation reactions at energies around the Coulomb barrier. The recoil products are identified either by the evaporated particles using charged-particle and neutron detectors or by their unique α or proton decay at the focal plane of a fragment separator like RITU [12] or the Fragment Mass Analyzer [13]. At GANIL, the use of the DIAMANT [14] and the NWALL [15] arrays coupled to the EXOGAM array led to a prolific detailed spectroscopy along the N=Z line in the vicinity of ^{100}Sn [16–20]. The development of the gas-filled mode of the VAMOS++ spectrometer will open new opportunities in the prompt spectroscopy of heavy and super-heavy elements [21,22]. Finally, in-beam γ-ray spectroscopy with post-accelerated radioactive beams from ISOL facilities like SPIRAL1 at GANIL, using nucleon transfer reactions in inverse kinematic or safe Coulomb excitation, are known to provide information of paramount importance for the understanding of these exotic beams. These techniques as used at GANIL will greatly benefit from the improved resolving power of a tracking array such as the AGATA 1π array [23].

The AGATA array was first implemented and operated at the INFN-Laboratori Nazionali di Legnaro (LNL) [24] and then at the final focal plane of the FRagment Separator (FRS) at the GSI facility [25–27]. The third implementation is at the GANIL facility, Caen -France, offering unique opportunities for high resolution in-beam γ-ray spectroscopy. The requirement of the installation of AGATA at GANIL was to be able to perform experiments covering a broad physics program, coupled to different ancillary detectors such as the VAMOS++ spectrometer [5,21], the EXOGAM [10], PARIS [28] and FATIMA [29,30] γ-ray spectrometers, the NWALL and NEDA neutron detectors [15,31–33], the DIAMANT [14] and GASPARD [34] charged-particle detectors as well as other detectors and devices which could be placed around the target position. The AGATA system at GANIL will consist of up to 45 capsules installed in 15 AGATA Triple Clusters (TC), later referred as the AGATA 1π array. In the present paper, we describe the conceptual design and installation of the AGATA 1π array at GANIL and detail several simulations showing the expected performances of the set-up in different configurations. The GANIL installation benefited from a major effort to commission the system and its performance will be detailed in a separated paper [35,36].

2. The AGATA 1π array installed at GANIL

The AGATA 1π array installed at GANIL consists of triple (TC) and possibly double (DC) clusters organized in a compact geometry of packed detectors to optimize the performance of the tracking array. The AGATA clusters are grouped at the most backward angles, symmetrically around the optical axis of to the VAMOS++ spectrometer. The general layout is presented in Fig. 1. This arrangement maximizes the peak-to-total ratio, the Doppler effect correction and the efficiency used for lifetime measurement. Indeed, thanks to the performances of both the Pulse Shape Analysis [24] and the Tracking algorithms [37,38], the whole solid angle covered by the AGATA clusters can be used for lifetime measurements based on the analysis of Doppler shifts. With respect to the LNL and GSI campaigns, the number of clusters was increased from 5 (7) clusters in the LNL (GSI) campaign respectively, to 15 clusters at GANIL. This increase of the number of channels led to the production of additional modules of the Detectors Support System [23] and the development of a second generation of Front-End and Back-End preprocessing electronics. In addition to the phase 1 electronics using the ATCA format described in Ref. [23], an advanced phase 1 electronics was designed. Following an important effort of integration, new digitizers (DIG-OPT12) were designed and produced [39]. These new digitizers have identical specifications with respect to the phase 1 digitizers while being three

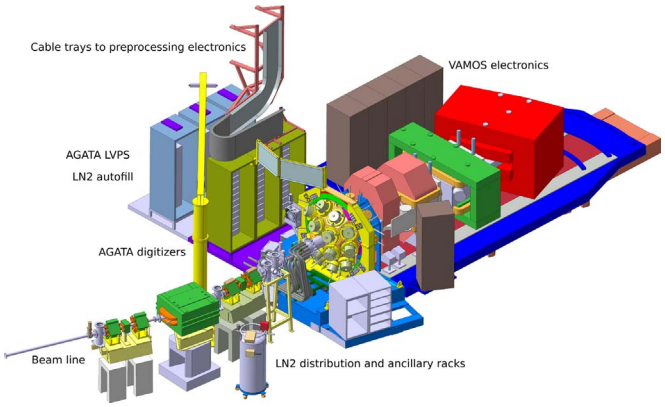

Fig. 1. (Color online) The AGATA 1π array at GANIL general layout in the G1 experimental hall.

times more compact and with a reduced power consumption. They use the same input signal cables and output optical links as the first generation of electronics, developed for the AGATA Demonstrator. The digital output is connected to a new pre-processing board (GGP) embedded in the AGATA servers, outside the experimental hall [40]. The GGP PCIe cards perform the data processing similarly to the ATCA carrier boards and is directly connected to the GTS tree [23], extended to cover the number of additional channels. The integration and validation of the coupling of both electronics phases were performed during the GANIL campaign. The advanced phase 1 electronics will complete the existing phase 1 up to 45 capsules at GANIL. The data acquisition infrastructure has also been upgraded with a new disk server using the CEPH technology [41] and a new network infrastructure with higher rate capabilities. A new distributed data acquisition system, DCOD, has also been implemented. This upgrade is a natural evolution of the NARVAL system [23,42] as a direct consequence of the array size increase.

3. Mechanical configuration and infrastructure

The AGATA 1π array is implemented in the G1 experimental hall at GANIL and placed at the target position of the VAMOS++ spectrometer. The Detectors Support System and the front-end electronics are installed close to the array (Fig. 1). On the bottom of the figure, two racks host the liquid nitrogen distribution and the electronics for the ancillary detectors installed at the target position. On the top part of the figure, the AGATA digitizers, the Low Voltage Power Supplies (LVPS) and the Liquid Nitrogen autofill systems are installed on a dedicated platform. Particular care was taken regarding the electromagnetic compatibility between the different platforms and the AGATA detector structure. Several measurements at different positions aiming to avoid grounding issues were performed during the mechanical assembly and shown results within the specifications. Cable trays for the signal cables from the detectors to the digitizers and for the optical links from the digitizers to the pre-processing electronics are visible next to the VAMOS++ electronics racks.

The AGATA 1π array holding structure (Figs. 2 and 3) and the VAMOS++ spectrometer are supported on a common platform which can rotate around a vertical axis perpendicular to the beam axis at the target position up to 45°. For the reaction products this makes the AGATA detectors angular position independent from the rotation of VAMOS++. The holding structure (Fig. 2) allows two additional degrees of freedom. The different axes are defined in the Fig. 4. The beam axis follows the $\vec{z}$ axis. First, the structure can be rotated by +/−90° around the beam axis in the $(\vec{x}, \vec{y})$ plane. This rotation is used for the installation of the AGATA cluster detectors which are always loaded in a unique horizontal position. Secondly, the distance between the target and the AGATA detectors can be adjusted within a millimetre precision. From the so-called nominal configuration (target to the front of the cryostat distance equal to 230 mm), the whole AGATA array can be translated towards the target by 100 mm and drawn back by 400 mm (see Fig. 5). The AGATA detectors positions (flanges) are organized as presented in Fig. 4. The beam axis, or the VAMOS++ spectrometer optical axis when used, is following the $\vec{z}$ axis. The labels indicate the flange number in the laboratory reference frame for the AGATA detectors and are identical to the LNL configuration [24]. The mechanical structure was re-assembled after the transfer from the GSI host laboratory. The convergence of the flanges, i.e. the projection on the $(\vec{x}, \vec{y})$ target plane of a line passing through the centre of each flange defining the common focal point of the flanges at the target position was accurately measured using laser trackers. The result of this projection for each flange is shown in Fig. 6. The first circle represents a tolerance of 100 μm, as the others are respectively 300 μm, 600 μm and 900 μm. All flanges are within 700 μm with respect to the centre, well below the specifications.

Even if the flanges are labelled as in the LNL campaign, we designed a rotation of −33.9° around the $\vec{z}$ axis, to allow the incoming beam line to pass through flange 1(8) for a platform rotation of nearly 20°(45°) respectively. An accurate measurement using laser trackers was performed after assembly in the experimental hall. The results are presented in Table 1 and Fig. 7. In the second column of Table 1, we indicate for each flange of Fig. 4 the polar angle (θ) with respect to the VAMOS++ spectrometer axis. The mechanical agreement is within 3×10^{-2} degrees according to the specifications. Similarly in the third column, the azimuthal angle (ϕ), in the $(\vec{x}, \vec{y})$ plane, is presented. An offset of −33.9°, consistent with the mechanical design of the present set-up, is found.

Thanks to the high precision of the laser tracked measurement, a detailed analysis can be done, providing valuable information for γ-ray tracking to obtain even more accurate positions. In Fig. 7, the difference in θ (top-black) and ϕ (bottom-black) between the AGATA specifications and the measurements is presented as a function of the flange number. The accuracy on the distance measurement using the laser tracker is 0.1 mm. A systematic offset in θ can be observed as a result of a wrong estimate along the $\vec{z}$ direction of the target point. In addition, a systematic geometrical de-orientation is revealed by the oscillation of the difference in both θ and ϕ angles as a function of the flange number. Corrections in the $\vec{z}$ direction of +315 μm and two rotations of −0.144 mrad in the $(\vec{x}, \vec{z})$ plane around the $\vec{y}$ axis and of +0.158 mrad in the $(\vec{y}, \vec{z})$ plane around the $\vec{x}$ axis give a better consistency as shown by the red points distributions in both plots.

Making use of the laser-tracker pre-installation in the experimental hall, allowing an accurate determination of the set-up geometry, each detector position was measured and aligned along the theoretical cluster axis defined by the central axis of each flange. The result is presented in Table 2. For each flange and each crystal type (A,B,C) [23], the distance from the target to the front of the cryostat end-cap is measured for AGATA placed at the nominal configuration (230 mm). The average measured distance is 231 mm with an average dispersion of 0.4 mm. It means that an offset of −1 mm should be applied in software in the data analysis. This accurate determination of the set-up geometry is motivated by the optimization of the Doppler correction. The Doppler broadening is today dominated by the position resolution of the tracking arrays (5 mm FWHM) and not by either the mechanical installation or the recoils momentum measurement in VAMOS++ as shown in [44]. As already mentioned, a compact configuration is possible by translating the complete structure by 100 mm toward the target. Fig. 5 presents the two configurations.

As the AGATA detectors are placed at the backward angles with respect to the VAMOS++ spectrometer optical axis, some angular range coverage and target to detectors distances are not possible due to mechanical interference between the detectors, or their support, and

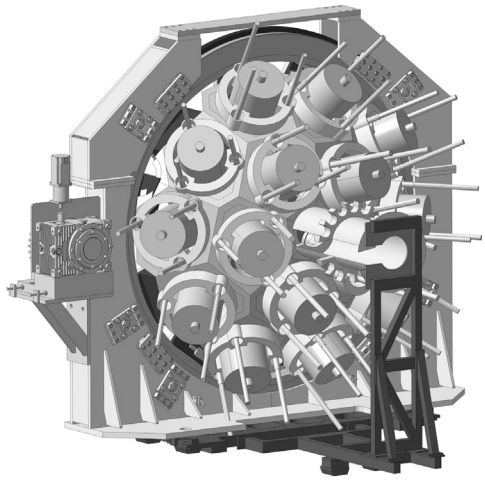

Fig. 2. The AGATA holding structure produced for the installation at GANIL.

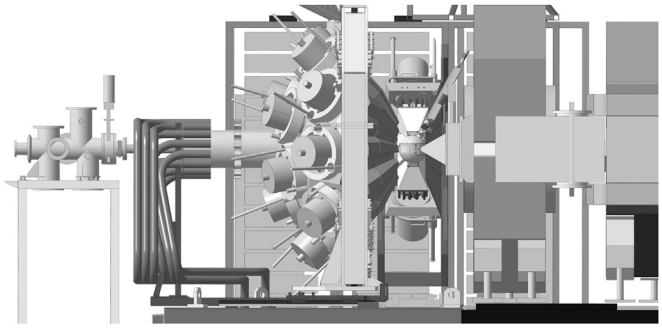

Fig. 3. Side view of the target position. The beam comes from the left. The AGATA 1π array is placed at the backward angles with respect to the beam direction. The AGATA holding structure is in nominal configuration (see text) coupled to EXOGAM clover detectors at 90° and the VAMOS++ spectrometer. The 62° target loader is used (see text) to allow the installation of the 8 EXOGAM clover detectors.

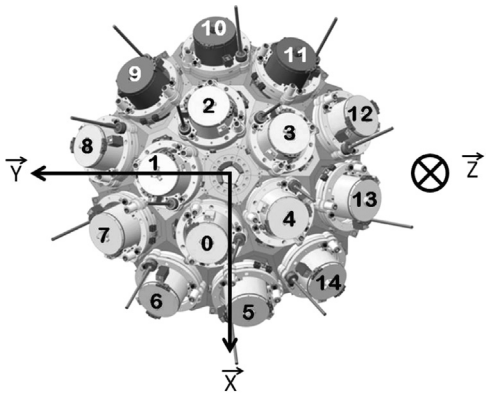

Fig. 4. The AGATA detector mechanical support at GANIL. The double clusters can be installed in positions 9, 10 and 11. The beam propagation is following the $\vec{z}$ axis. The ϕ angle is defined from the $\vec{x}$ axis, clockwise.

the incoming beam tube. The available combinations of angles and distances are summarized in Tables 3, 4. The first column indicates the angle between the beam and the VAMOS++ axis, and the second and third columns indicate the closest and largest available distances respectively with respect to the nominal configuration (230 mm). At 0°, all distances up to the compact configuration are available. Between 1° and 9° and between 33° and 40°, there is a mechanical incompatibility with the beam tube. For angles between 10° and 18°, and angles between 41° and 45°, no detector can be placed in flange 1 and 8 respectively due to the presence of the beam pipe. In the remaining ranges, the most compact configuration is determined before mechanical interference between the beam tube and the flange or the detector

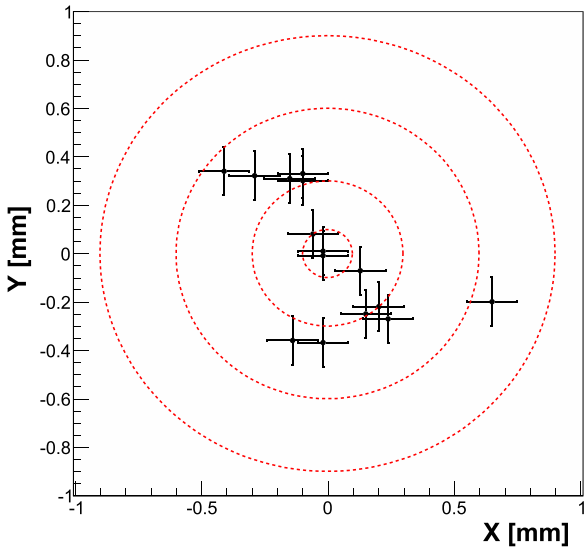

Fig. 6. (Color online) Projection on the target plane of the focusing point of each flange. (see text).

Table 1
Measured θ and ϕ angles in degrees of the AGATA flanges at GANIL.

Flange	θ_{meas}	ϕ_{meas}
0	158.032(6)	10.01(1)
1	158.046(6)	82.01(1)
2	158.058(6)	154.02(1)
3	158.033(6)	226.01(1)
4	158.031(6)	298.00(1)
5	134.715(6)	−16.21(1)
6	131.674(6)	20.92(1)
7	134.720(6)	55.78(1)
8	131.682(6)	92.92(1)
9	134.734(6)	127.79(1)
10	131.695(6)	164.92(1)
11	134.726(6)	199.79(1)
12	131.677(6)	236.93(1)
13	134.709(6)	271.78(1)
14	131.668(6)	308.92(1)

cryostat.

3.1. Target loader and reaction chamber

Specific target chambers and loader were designed to cover most of the physics cases including the use of fragile thin targets and lifetime measurements using a plunger device. In the latter case, the target

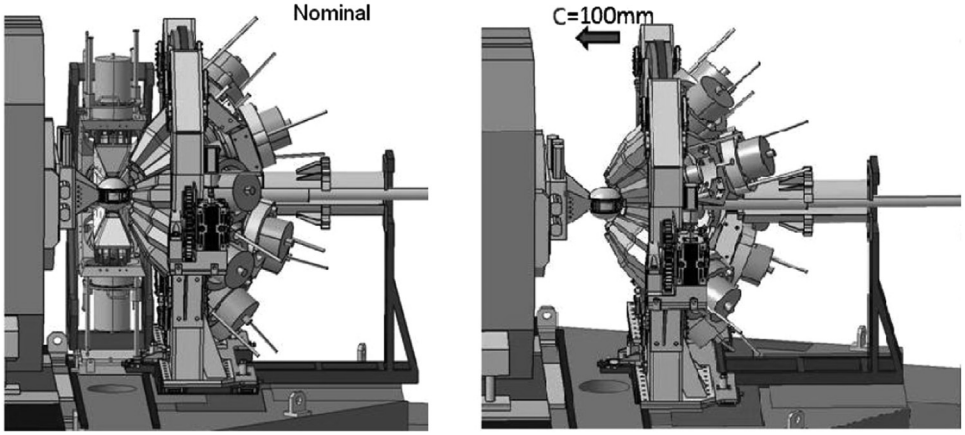

Fig. 5. *Left:* AGATA in the nominal configuration coupled to the EXOGAM detector. *Right:* AGATA in the compact configuration without ancillary detectors in the 90° ring.

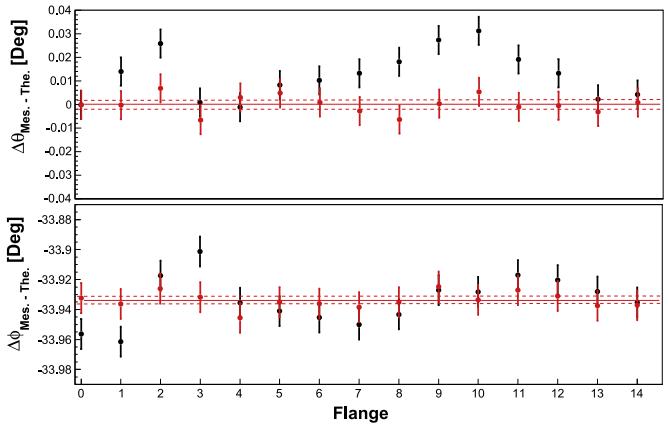

Fig. 7. (Color online) *Top:* Difference in θ angle between the theoretical position [43] and the measurement in degrees, before (black) and after (red) corrections. *Bottom:* Same for the ϕ angle.

Table 2
Target to-front-of-cryostat distance in millimetre for each AGATA detector present in the array at the time of the measurement.

F0-A	231.6(1)	F0-B	231.5(1)	F0-C	231.3(1)
F2-A	230.3(1)	F2-B	230.6(1)	F2-C	230.8(1)
F3-A	230.3(1)	F3-B	230.6(1)	F3-C	230.7(1)
F4-A	230.6(1)	F4-B	230.6(1)	F4-C	230.5(1)
F10-A	231.9(1)	F10-B	231.9(1)	F10-C	231.2(1)
F11-A	231.3(1)	F11-B	230.6(1)	F11-C	230.6(1)
F12-A	231.0(1)	F12-B	231.0(1)	F12-C	230.5(1)
F13-A	231.0(1)	F13-B	231.0(1)	F13-C	231.2(1)
Average	230.9	Ave. Dev.	0.4		

Table 3
Available ranges for the AGATA translation along the $\vec{z}$ axis relative to the nominal configuration (0 mm), as a function of the AGATA-VAMOS angle with respect to the incoming beam tube. Negative (positive) values correspond to AGATA translation towards (away from) VAMOS++. The AGATA translation for the minimum (maximum) available target-AGATA distance is given in column 2 (3). A positive value in column 2 indicates that the closest distance is larger than the nominal. On the contrary a negative value in column 3 indicates that the largest distance is closer than the nominal. Angles are expressed in degrees while distances are expressed in millimetres.

Angle	Translation for minimum target-AGATA distance	Translation for maximum target-AGATA distance	Comment
0	−100	360	Nominal to compact available
1–2	–	–	Interference with detector in F2
3–9	–	–	Interference with the Honeycomb
10	345	360	F1 empty. Nominal unavailable
11	230	360	”
12	135	360	”
13	100	360	”
14	75	360	”
15	50	360	”
16	35	360	”
17	20	360	”
18	5	360	”
19	−10	360	F1 empty. Nominal available
20	−20	360	”
21	−30	360	”
22	−40	345	”
23	−50	260	”
24	−57	210	”
25	−65	165	”
26	−70	125	”

Table 4
Same as Table 3 for larger angles.

Angle	translation for minimum target-AGATA distance	translation for maximum target-AGATA distance	Comment
27	−76	85	”
28	−84	48	”
29	−88	5	”
30	−93	−30	F1 empty. Nominal unavailable
31	−98	−65	”
32	−100	−100	”
33	220	360	F8 empty. Nominal unavailable
34	180	360	”
35	150	360	”
36	120	360	”
37	90	360	”
38	65	360	”
39	36	360	”
40	10	360	”
41	−15	340	F8 empty. Nominal available
42	−36	315	”
43	−60	290	”
44	−80	265	”
45	−100	240	”

loader is excluded. The target chamber is connected to the VAMOS++ spectrometer and to the accelerator beam line by a narrow beam tube (42.3 mm diameter) passing through empty AGATA detector positions. The chamber is large enough to host a plunger device [45,46] and to cope with the compact configuration. A first target chamber is presented with the target loader in Fig. 8 and with the Cologne plunger [45] in Fig. 9 for the use of VAMOS++ in vacuum mode. The chamber consists of three independent pieces: the central piece is constituted by a cylindrical part and a conical part, allowing the connection to the VAMOS++ vacuum chamber, while two independent hemispheres, at the top and the bottom, close the chamber. These hemispheres can be adapted to any configuration. Two full hemispheres were produced to close the chamber when the plunger is used and two hemispheres with a hole at 90° and 62° with respect to the VAMOS++ optical axis were produced to connect different target loaders. A second specific target chamber, 2 mm Al thick, was produced for the coupling of AGATA with the NEDA/NWALL and DIAMANT arrays. It includes also the possibility to use a plunger device coupled to the DIAMANT array and the target loader.

The remotely controlled target loader hosts five targets and consists of an independent vacuum chamber (top part in Fig. 8) which can be connected to or disconnected from the target chamber, without pumping down the vacuum in the latter. The independent chamber allows the mounting of fragile targets in a protected atmosphere. This target holder can be adapted to any target chamber design for AGATA at GANIL.

4. Local infrastructure

Particular attention was paid to the permanent supply of liquid nitrogen (LN2) and the corresponding monitoring. The AGATA clusters must remain at the liquid nitrogen temperature without any interruption over the whole AGATA campaign. At GANIL, the automatic refill and control is performed through the AGATA DSS system [23] whereas the liquid nitrogen delivery and distribution is provided by the GANIL local infrastructure. An intermediate buffer tank of 220 liters of liquid nitrogen is equipped with a manifold feeding up to eight AGATA clusters. For the complete AGATA 1π array, two independent systems with two buffer tanks have been installed. The monitoring of the temperature is performed without interruption via an automatic

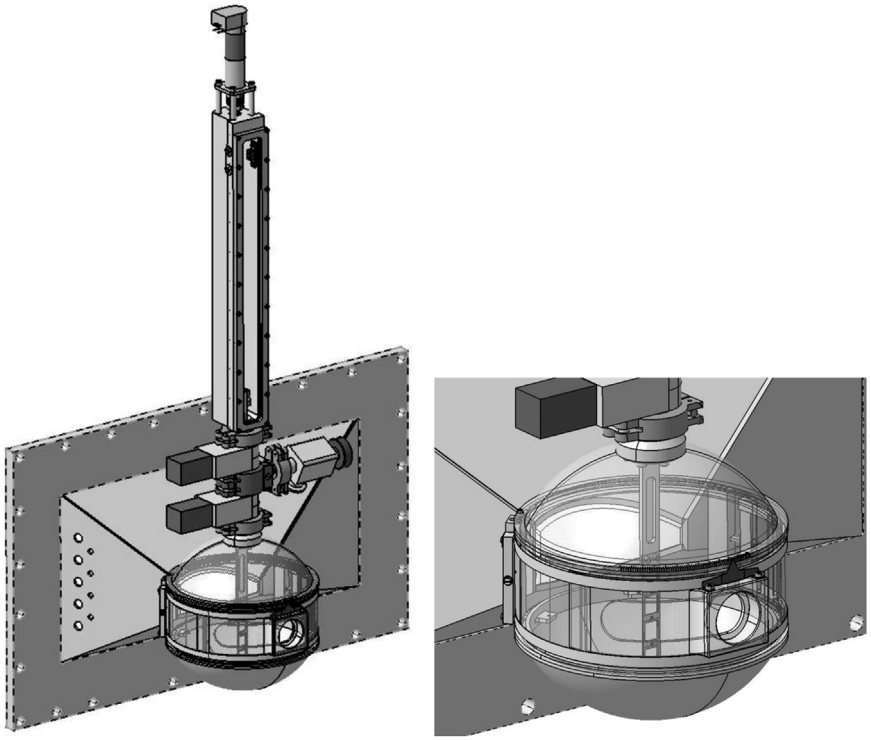

Fig. 8. *Left:* View of the standard AGATA-VAMOS target chamber with its target loader in an independent vacuum chamber. The large plate connects the chamber to the VAMOS++ first quadrupole chamber.*Right:* Zoom on the chamber containing five targets.

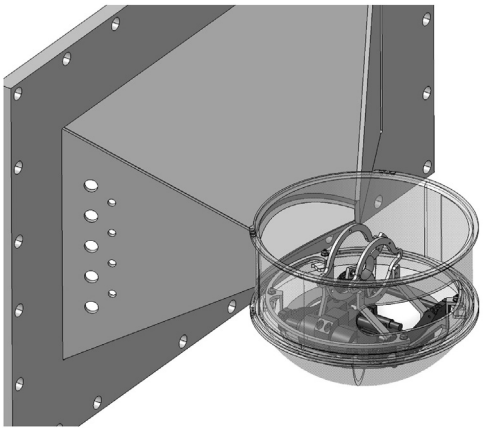

Fig. 9. View of the standard AGATA-VAMOS target chamber with the Cologne plunger.

system allowing emergency refills and the automatic shut-down of non-vital elements of the AGATA clusters, keeping as highest priority the permanent supply of liquid nitrogen. The automatic filling system, based on the MUSCADE product [47], can be accessed through a VPN connection by a team in charge of its monitoring. In addition, an alarm system generates a text message with error report in case of a problem. The power distribution for the front-end electronics and the pre-amplifiers is provided by the AGATA DSS system integrating the detector survey [23] through the secured GANIL facility power plant. The cooling of the front-end electronics is ensured by cold water at 18.5° at a pressure of 5 bars with a flow of 11 m^3/h.

5. Ancillary detectors

As stated in the introduction, the AGATA campaign aims at benefiting from the large palette of stable and radioactive beams delivered by the GANIL facility but also from a large set of spectrometers and particle detectors. The AGATA 1π array can be coupled to the VAMOS++ magnetic spectrometer in vacuum mode [5,44] or in its future gas-filled mode [21]. As shown in Fig. 5, mechanical structures can be inserted between the VAMOS++ entrance and AGATA placed in the nominal configuration. In this figure, the EXOGAM frames are installed allowing the coupling with EXOGAM clover detectors or with other γ-ray spectrometers such as the FATIMA [29,30] or PARIS [28] $LaBr_3$ scintillators.

The VAMOS++ spectrometer can also be translated away by 1.1 m allowing the possibility of inserting a larger system such as the NEDA [31–33] and NWALL [15] neutron detectors as presented in Fig. 10. AGATA is shown in compact configuration in the figure. The coupling of AGATA with neutron and charged-particle detectors such as DIAMANT [14] or GASPARD [34], or large scintillator detectors for γ-rays, will be part of the AGATA campaign at GANIL.

One of the critical issues when coupling the data flow of AGATA with complementary instrumentation is the synchronization of both electronics. The electronics coupling is done by the time-stamp and the trigger decision distributed by the GTS system [48] via the VME AGAVA board [23] or directly integrated in the EXOGAM2, NEDA/

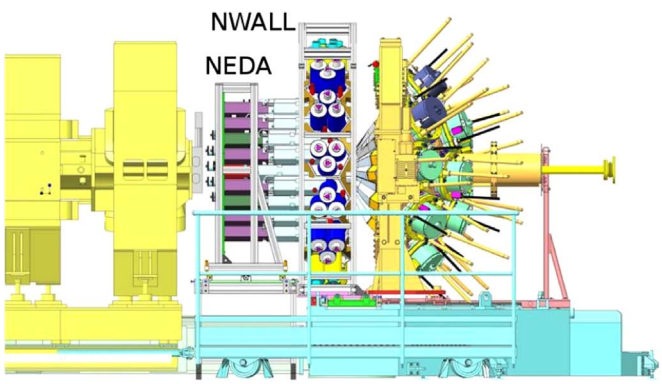

Fig. 10. (Color online) AGATA coupled to the NEDA and NWALL detectors with the VAMOS spectrometer translated by 1.1 m downstream.

NWALL and DIAMANT back-end electronics. A fully integrated data-flow management between the ancillary detectors and the AGATA Narval-DCOD data-flow [42] is provided and presented in Fig. 11. The ancillary detectors use the GANIL Narval data flow (GANIL Narval Topology in Fig. 11). These data are simultaneously stored on the local GANIL disk infrastructure and sent by TCP/IP to a dedicated work-station connected both to the GANIL and AGATA networks. The MFM2ADF Narval actors in the AGATA system collect the GANIL buffers in the MultiFrame Metaformat (MFM) [49], ensure a conversion to the AGATA Data Flow (ADF) format [23] and write the GTS time-stamp in the event header to ensure a proper event merging. The clock distribution is ensured by the AGATA GTS-ROOT mezzanine board and the trigger decision by the AGATA Trigger Processor [23,48]. The GANIL Run Control Core (RCC) [50] manages the ancillaries readout as well as the GANIL Narval actors for data collection and writing, and AGATA local and global level processing Narval actors [23]. The RCC manages experiment and run identifications for both AGATA and GANIL systems. The connection between the GANIL and AGATA environments is ensured by the Global Control Core (GCC) software bridge. A ROOT-based [51] data-analysis package handling both AGATA and GANIL data has been produced [23,52].

6. AGATA simulations

The expected performance of the AGATA 1π array have been simulated using the AGATA Geant4 package [43]. Photo-peak efficiencies and peak-to-total ratios as a function of the γ-ray energy have been investigated. The AGATA Geant4 modelling has been continuously improved. Constrained from source measurements have been taken into account and new ancillary detectors and a realistic target chamber description are included using the *gdml* extension of Geant4 [53]. Comparison of simulated and measured efficiencies of the AGATA array installed at GSI was published in [27]. It shows reasonable discrepancies between measurement and simulation. At GANIL, the absolute photopeak efficiency on the total projection of the core energy, for the 1.408 MeV γ-ray from the ^{152}Eu source and for 24 capsules (8 Triple Cluster during the 2015 run) at the nominal position, was measured to 2.34(1)%. The simulated value is 2.64% with a similar agreement to the measurement as [27]. In the present paper, the simulations were performed with AGATA placed at both the nominal and compact position for a complete 1π array. Efficiencies were calculated using the core energy and the calorimetric energy (sum of all energies deposited in AGATA), and after tracking using the MGT code with standard parameters [37]. Interaction points from the simulation are not determined by the Pulse Shape Analysis using the adaptive grid search as done from detector signals but packed within 5 mm. The photo-peak efficiency can be estimated analytically as a function of the γ-ray energy using the formula:

$$\epsilon_\gamma(E) = e\left(\sum_{i=0}^{4} P_i (ln(E))^i\right) \quad (1)$$

where E is the γ-ray energy in keV and the P_i parameters are given for each configuration.

Fig. 12 presents the photo-peak efficiency of AGATA 1π as a function of the γ-ray energy for both nominal and compact configurations. The photo-peak efficiency at 1.3 MeV of the ^{60}Co source, simulated at multiplicity equal 1, is 8.3% (15.3%) in nominal (compact) position respectively using the calorimetric energy. The P_i parameters are given in Table 5 for each configuration.

Fig. 13 presents the photo-peak efficiency of AGATA 1π as a function of the γ-ray energy after tracking for both nominal and compact configurations. The photo-peak efficiency at 1.3 MeV of the ^{60}Co source is 8.1% (14.8%) in nominal (compact) position, respectively. The P_i parameters are given in Table 6.

The impact on the Doppler broadening in the compact configuration with respect to the nominal configuration was also investigated in the range of the typical velocities for recoils produced using deep inelastic collisions, fusion-fission and fusion-evaporation reactions. Fig. 14 presents the relative resolution as a function of the recoil velocity for both the nominal and the compact configurations. At 15% speed of light, an increase of 25% and 60% of the FWHM is predicted by the simulation with respect to a γ-ray emitted at rest in the nominal and the compact configuration respectively. The uncertainties on the recoil momentum are not taken into account in this evaluation. The Doppler broadening obtained in in-beam commissioning for recoil having v/c $\simeq$10% shown in [44,35] is therefore slightly above the simulated values. One should take care in the case of a lifetime measurement that the Doppler shift between the slow and fast component remains sufficient over the whole solid angle and is not dominated by the Doppler broadening.

Simulations were performed when the NWALL [15] and the DIAMANT [14] arrays are placed in the set-up. The NEDA array geometry detailed in Ref. [31–33] is not yet fully implemented in the standard package. The DIAMANT array, placed around the target in a dedicated vacuum chamber (Section 3.1), will impact the AGATA 1π photo-peak efficiency and the peak-to-total ratio due to the absorption and the Compton scattering in the CsI cells. On the contrary, the NWALL array placed in the forward direction will not influence the AGATA photo-peak efficiency. However, since the AGATA detectors are not collimated, it will still decrease the peak-to-total ratio due to mutual Compton backscattering between the two arrays. As the NEDA and NWALL arrays are covering a similar solid angle [31–33] and are using the same liquid scintillator for the neutron detection, the present simulation remains a reasonable assumption. The following simulations present the different configurations with related efficiencies and peak-to-total ratio. The peak-to-total ratio is calculated with a low energy threshold of 20 keV in the AGATA crystal.

First, we present in Fig. 15 the photo-peak efficiency and the peak-to-total ratio, using the calorimetric energy, of the AGATA 1π array as a function of the γ-ray energy in the compact configuration when

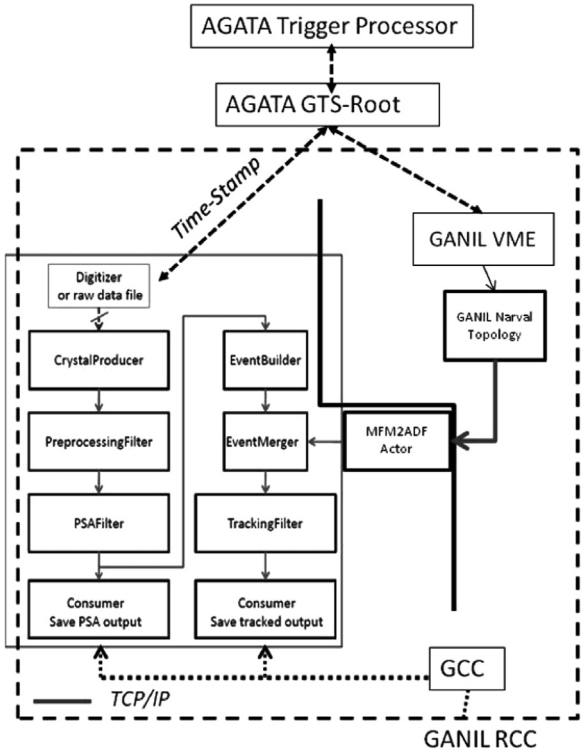

Fig. 11. AGATA data-flow topology combining both AGATA and GANIL Narval actors, Global Control Core (GCC) and Run Control Core (RCC) sub-systems.

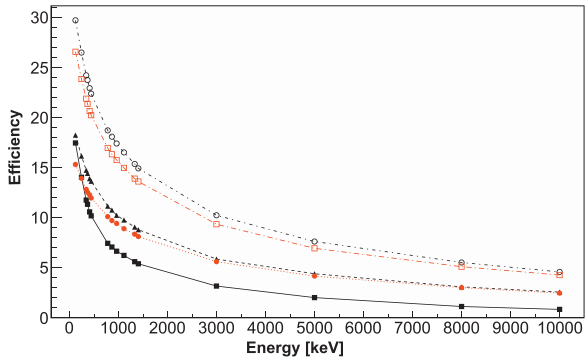

Fig. 12. (Color online) Simulated photo-peak efficiency of AGATA 1π as a function of the γ-ray energy. The full (open) symbols correspond to AGATA placed in nominal (compact) position, respectively. The full black squares correspond to the sum of the core without target chamber. The full black triangles correspond to the calorimetric energy efficiency without target chamber. The full red circles include the target chamber. The open black circles correspond to the calorimetric energy efficiency in compact configuration including the target chamber. The open red squares include the Lorentz boost originating from an in-flight emission with β=0.1.

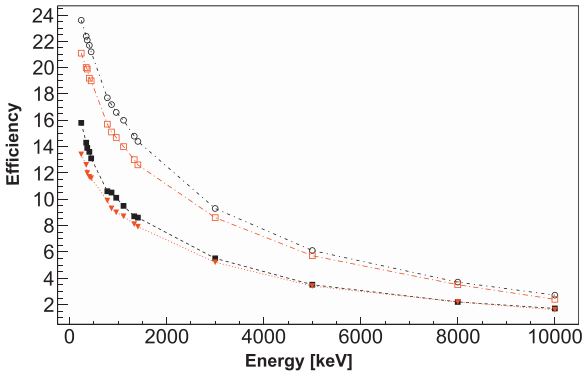

Fig. 13. (Color online) Simulated photo-peak efficiency of AGATA 1π as a function of the γ-ray energy after tracking (MGT). The full (open) symbols correspond to AGATA placed in nominal (compact) configuration respectively. The full black squares correspond to the efficiency after tracking without target chamber. The full red triangles show the efficiency including the target chamber. The open black circles correspond to the compact configuration with the target chamber. The open red squares include the boost originating from an in-flight emission with β=0.1.

DIAMANT is placed or not at the target position. The reduced efficiency for low energy γ-ray, arising from the absorption in the DIAMANT CsI cells, is clearly visible. The photo-peak efficiency at the 121 keV ^{152}Eu source line is reduced by 60% and by 10% at 1.3 MeV ^{60}Co source γ-ray energies. The P_i parameters are given in Table 7. Similarly, the peak-to-total ratio is reduced with the use of the DIAMANT array, in particular for low energy γ-rays.

Secondly, the photo-peak efficiency and peak-to-total ratio, in the nominal configuration, using the calorimetric energy and calculated after γ-ray tracking (MGT) are presented in Fig. 16 for the low energy part, where the effect of DIAMANT CsI cells is the most significant. Similarly, a reduced efficiency is obtained at low energy when DIAMANT is used. One can notice that the photo-peak efficiency and peak-to-total ratio between the calorimetric energy and after the γ-ray tracking are relatively independent from the use of DIAMANT or not in the set-up. A better peak-to-total ratio is consistently obtained after γ-ray tracking with respect to the calorimetric energy spectrum. The corresponding P_i parameters are given in Table 8.

In order to detail the contribution to the Compton scattering background originating from the different complementary detectors, the γ-ray spectrum is further analysed in Fig. 17 for a 460 keV γ-ray transition and in Fig. 18 for a 1332 keV γ-ray transition. The black spectrum is the total projection. The photo-peak, the Compton edge and the backscattering peaks are visible. The red spectrum corresponds to events in which no γ-ray was detected in both the NWALL and the DIAMANT arrays. These events represent 85% of the total events in the AGATA array. Both the Compton edge and the backscattering peaks are significantly reduced. The yellow spectrum, representing 6% of the events, is the AGATA γ-ray spectrum in coincidence with at least one γ-ray scattering in the NWALL covering the 1π forward solid angle. The spectrum is dominated by the Compton edge and the backscattering peaks. They correspond either to a backscattering from AGATA to the NWALL or vice-versa. The blue spectrum, representing also 6% of the AGATA events, is the AGATA γ-ray spectrum in coincidence with at least one γ-ray scattering in the DIAMANT array surrounding the target. As DIAMANT is nearly a 4π array, the spectrum covers a large range in energy lower than the photo-peak and is slightly shifted towards higher energies, with respect to standard partial absorption spectra, as the first interaction occurs in DIAMANT before interaction

Table 6
Parameters associated to the simulated AGATA (1π) photo-peak efficiency curves: (A) In nominal configuration after tracking (MGT) without the target chamber. (B) Same as (A) with the target chamber. (C) Same as (B) in compact configuration. (D) Same as (C) with a β=0.1 boost.

Parameter	A	B	C	D
p0	7.43304	2.18729	−14.545	−15.0357
p1	−1.58216	1.16825	10.7319	10.9954
p2	0.128429	−0.435597	−2.40663	−2.46268
p3	0.00835408	0.0604216	0.240487	0.244599
p4	−0.00135935	−0.00315858	−0.00931915	−0.0093787

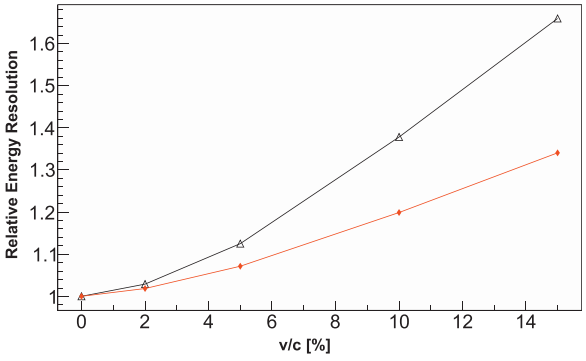

Fig. 14. (Color online) Simulated relative resolution after tracking and Doppler correction for the nominal (compact) position in full red (open black) symbols, respectively, as a function of the recoil velocity v/c.

Table 5
Parameters associated to the simulated AGATA (1π) photo-peak efficiency curves: (A) In nominal configuration, sum of the core energy, without the target chamber. (B) Same as (A) with the calorimetric energy. (C) Same as (B) with a realistic target chamber. (D) Same as (C) in compact configuration. (E) Same as (D) with a β=0.1 boost.

Parameter	A	B	C	D	E
p0	−29.5054	−2.76666	−2.24011	−0.896561	−1.27209
p1	20.8338	3.56035	3.11882	2.76527	2.89501
p2	−4.8688	−0.786507	−0.695035	−0.622822	−0.645484
p3	0.492352	0.0741596	0.0670646	0.0598514	0.0615096
p4	−0.0186652	−0.00282175	−0.00264335	−0.00236008	−0.00239715

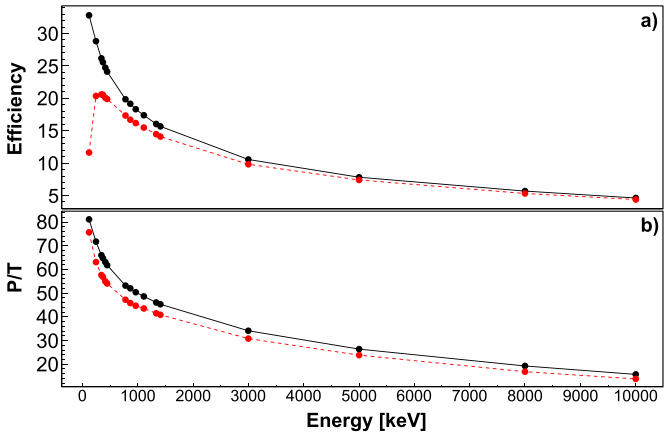

Fig. 15. (Color online) a) Simulated photo-peak efficiency of the AGATA 1π array in the compact configuration as a function of the γ-ray energy for the NWALL/DIAMANT set-up using the calorimetric energy. The black (red) symbol corresponds to the results without (with) the DIAMANT array at the centre, respectively. b) Similar results for the peak-to-total ratio.

Table 7
Parameters associated to the AGATA (1π) photo-peak efficiency curves: (A) In the compact configuration without target chamber using the calorimetric energy. (B) Same as (A) with the DIAMANT array at the target position.

Parameter	A	B
p0	−1.23426	−65.8794
p1	3.05212	38.2521
p2	−0.686427	−7.87019
p3	0.0654242	0.714594
p4	−0.00253284	−0.0244152

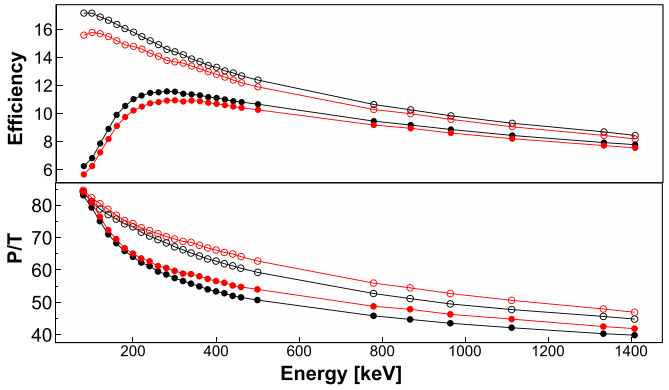

Fig. 16. (Color online) *Top:* Simulated photo-peak efficiency of AGATA 1π array in the nominal configuration as a function of the γ-ray energy for the NWALL/DIAMANT set-up. The full symbols correspond to a configuration including the NWALL and the DIAMANT arrays. The open symbols correspond to configuration without ancillary detectors. The black and red symbols correspond to the results with respectively the calorimetric energy and after tracking. *Bottom:* Same for the peak-to-total ratio.

Table 8
Parameters associated to the simulated AGATA (1π) photo-peak efficiency curves: (A) In the nominal configuration without the DIAMANT array and using the calorimetric energy. (B) Same as (A) after tracking (MGT). (C) Same as (A) with the DIAMANT array. (D) Same as (C) after tracking (MGT).

Parameter	A	B	C	D
p0	−2.27055	0.165478	−12.5339	8.90561
p1	2.94882	1.17116	4.33303	−10.5715
p2	−0.577703	−0.127785	0.170537	3.9884
p3	0.0449852	−0.00342125	−0.136784	−0.565892
p4	−0.00135621	0.000533228	0.00953563	0.0274318

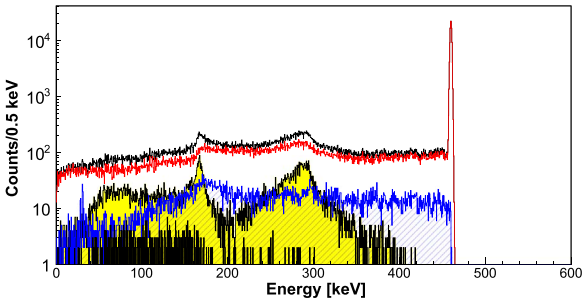

Fig. 17. (Color online) Simulated detailed contribution to the Compton background in AGATA 1π in the nominal configuration for a 460 keV γ-ray transition using the calorimetric energy. Black: total projection. Red: anti-coincidence with the NWALL and the DIAMANT arrays. Yellow: anti-coincidence with the DIAMANT array and in coincidence with a γ-ray event in the NWALL array. Blue: anti-coincidence with the NWALL array and in coincidence with a γ-ray event in the DIAMANT array. Filled black: triple coincidence between the AGATA, NWALL and DIAMANT arrays.

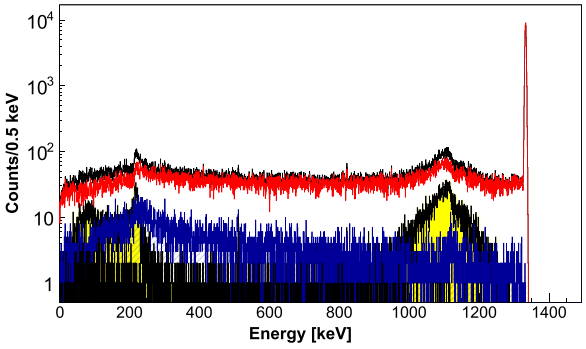

Fig. 18. (Color online) Same as Fig. 17 for 1332 keV γ-ray transition.

with the AGATA Ge crystals. The filled black spectrum corresponds to a triple coincidence between AGATA, the NWALL and the DIAMANT arrays and represents less than 1% of the events.

The impact of the DIAMANT and the NWALL arrays on the AGATA 1π array photo-peak efficiency and peak-to-total is clearly demonstrated in Figs. 15 and 16. We propose to evaluate the impact on the tracking efficiency itself as a function of the γ-ray energy and source multiplicity. Events at different γ-ray energies between 200 keV and 2 MeV are generated in a cascade of 1, 5 or 10 simultaneous transitions. Simulations are performed in the nominal and the compact configurations. First, an efficiency using the calorimetric energy is determined for each γ-ray energy for both distances and in source multiplicity equal to 1, with and without the DIAMANT and NWALL arrays. These efficiency values are used as individual responses of the array, hence including the absorption in the DIAMANT cells when used. Then, for each point in Fig. 19, the photo-peak efficiency after

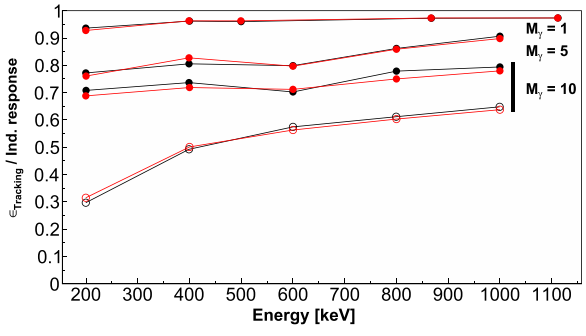

Fig. 19. (Color online) Simulated tracking efficiency of AGATA 1π in the nominal configuration as a function of the γ-ray source multiplicity and energy, for a configuration without ancillary detectors (black) and coupled to the DIAMANT and NWALL arrays (red). The open symbols correspond to the compact configuration.

tracking (MGT) is determined and normalised to the individual response. The black points are calculated without ancillary detectors whereas the NWALL and the DIAMANT arrays are used for the red points. At multiplicity 1 ($M_\gamma = 1$), the tracking efficiency is ~95% as a function of the γ-ray energy, independently if DIAMANT is used or not.

By increasing the source multiplicity up to 10 ($M_\gamma = 10$), the tracking efficiency decreases as expected and is further reduced in the compact configuration (open symbols). A negligible effect is visible when DIAMANT is used or not, within the simulation error, at higher multiplicity in both compact and nominal configurations. As a conclusion, the DIAMANT array, surrounding the target, does not affect the tracking algorithm efficiency in the energy range considered in the present simulation. This effect is consistent with the fact that the Rayleigh scattering cross section through the DIAMANT array is negligible for γ-rays energies above ~100 keV thanks to the relatively small thickness of the CsI cells.

7. Conclusion

The AGATA 1π array is currently being implemented at the GANIL SPIRAL2 facility. All the infrastructure, electronics and DAQ items are installed for up to 45 crystals (1π of the solid angle) and working according to specifications. The number of AGATA capsules available for experiments is regularly increasing as a function of delivery. The physics campaign started in 2015 and will continue to at least until end of 2019 with AGATA coupled to other detectors like NEDA/NWALL and DIAMANT, $LaBr_3$ scintillator (PARIS, FATIMA), VAMOS gas-filled mode and charged particle detector like MUGAST. The scientific campaign offers large opportunities using the stable and radioactive beams from the GANIL facility. The conceptual design was done in such a way that from a unique integration a very broad physics program associated to the use of a large variety of ancillary detectors and spectrometers can be performed. The GANIL installation offers a large flexibility with complete software and hardware integration. The mechanical and infrastructure installations were accurately controlled and fit the expectations. Mechanical constraints have been clearly identified and the present article describes the opportunities offered to a large user community.

Acknowledgements

The authors would like to acknowledge for its support the European Union, Seventh Framework Programme through ENSAR, Contract No. 262010. This project has received funding from the European Union's Horizon 2020 research and innovation programme under grant agreement No 654002. A.G., was partially supported by MINECO and Generalitat Valenciana, Spain, under the Grants FPA2014-57196-C5 and PROMETEOII/2014/019, and by the EU FEDER funds.

References

[1] R. Broda, C.T. Zhang, P. Kleinheinz, R. Menegazzo, K.-H. Maier, H. Grawe, M. Schramm, R. Schubart, M. Lach, S. Hofmann, Collisions between ^{106}Cd and ^{54}Fe at 30 mev above the coulomb barrier by high resolution $\gamma\gamma$ coincidences, Phys. Rev. C 49 (1994) R575–R579. http://dx.doi.org/10.1103/PhysRevC.49.R575 (URL ⟨http://link.aps.org/doi/10.1103/PhysRevC.49.R575⟩).

[2] R. Broda, High-spin states in neutron-rich nuclei explored with deep-inelastic hi reactions, Eur. Phys. J. A 13 (2002) 1–4.

[3] D. Bazin, J. Caggiano, B. Sherrill, J. Yurkon, A. Zeller, The {S800} spectrograph, Nuclear Instruments and Methods in Physics Research Section B: Beam Interactions with Materials and Atoms, in: Proceedings of the 14th International Conference on Electromagnetic Isotope Separators and Techniques Related to their Applications, 204 2003, pp. 629–633. http://dx.doi.org/10.1016/S0168-583X(02)02142-0. URL ⟨//www.sciencedirect.com/science/article/pii/S0168583×02021420⟩.

[4] A. Stefanini, L. Corradi, G. Maron, A. Pisent, M. Trotta, A. Vinodkumar, S. Beghini, G. Montagnoli, F. Scarlassara, G. Segato, A.D. Rosa, G. Inglima, D. Pierroutsakou, M. Romoli, M. Sandoli, G. Pollarolo, A. Latina, The heavy-ion magnetic spectrometer {PRISMA}, Nuclear Physics A 701, 120134, 2002, pp. 217–221, in: Proceedings of the 5th International Conference on Radioactive Nuclear Beams. http://dx.doi.org/10.1016/S0375-9474(01)01578-0.

[5] M. Rejmund, B. Lecornu, A. Navin, C. Schmitt, S. Damoy, O. Delaune, J. Enguerrand, G. Fremont, P. Gangnant, L. Gaudefroy, B. Jacquot, J. Pancin, S. Pullanhiotan, C. Spitaels, Performance of the improved larger acceptance spectrometer: vamos++, Nucl. Instrum. Methods Phys. Res. Sect. A: Accel., Spectrometers, Detect. Assoc. Equip. 646 (1) (2011) 184–191. http://dx.doi.org/10.1016/j.nima.2011.05.007.

[6] W. Mueller, J. Church, T. Glasmacher, D. Gutknecht, G. Hackman, P. Hansen, Z. Hu, K. Miller, P. Quirin, Thirty-two-fold segmented germanium detectors to identify γ-rays from intermediate-energy exotic beams, Nucl. Instrum. Methods Phys. Res. Sect. A: Accel., Spectrometers, Detect. Assoc. Equip. 466 (3) (2001) 492–498. http://dx.doi.org/10.1016/S0168-9002(01)00257-1 (URL ⟨//www.sciencedirect.com/science/article/pii/S0168900201002571⟩).

[7] S. Paschalis, I. Lee, A. Macchiavelli, C. Campbell, M. Cromaz, S. Gros, J. Pavan, J. Qian, R. Clark, H. Crawford, D. Doering, P. Fallon, C. Lionberger, T. Loew, M. Petri, T. Stezelberger, S. Zimmermann, D. Radford, K. Lagergren, D. Weisshaar, R. Winkler, T. Glasmacher, J. Anderson, C. Beausang, The performance of the gamma-ray energy tracking in-beam nuclear array {GRETINA}, Nucl. Instrum. Methods Phys. Res. Sect. A: Accel., Spectrometers, Detect. Assoc. Equip. 709 (2013) 44–55. http://dx.doi.org/10.1016/j.nima.2013.01.009 (URL ⟨//www.sciencedirect.com/science/article/pii/S0168900213000508⟩).

[8] D. Weisshaar, D. Bazin, P. Bender, C. Campbell, F. Recchia, V. Bader, T. Baugher, J. Belarge, M. Carpenter, H. Crawford, M. Cromaz, B. Elman, P. Fallon, A. Forney, A. Gade, J. Harker, N. Kobayashi, C. Langer, T. Lauritsen, I. Lee, A. Lemasson, B. Longfellow, E. Lunderberg, A. Macchiavelli, K. Miki, S. Momiyama, S. Noji, D. Radford, M. Scott, J. Sethi, S. Stroberg, C. Sullivan, R. Titus, A. Wiens, S. Williams, K. Wimmer, S. Zhu, The performance of the γ-ray tracking array {GRETINA} for γ-ray spectroscopy with fast beams of rare isotopes, Nuclear Instruments and Methods in Physics Research Section A: Accelerators, Spectrometers, Detectors and Associated Equipment (2016) – http://dx.doi.org/10.1016/j.nima.2016.12.001 URL ⟨//www.sciencedirect.com/science/article/pii/S0168900216312402⟩.

[9] A. Gadea, D.R. Napoli, G. de Angelis, R. Menegazzo, A.M. Stefanini, L. Corradi, M. Axiotis, L. Berti, E. Fioretto, T. Kroell, A. Latina, N. Marginean, G. Maron, T. Martinez, D. Rosso, C. Rusu, N. Toniolo, S. Szilner, M. Trotta, D. Bazzacco, S. Beghini, M. Bellato, F. Brandolini, E. Farnea, R. Isocrate, S.M. Lenzi, S. Lunardi, G. Montagnoli, P. Pavan, C. Rossi Alvarez, F. Scarlassara, C. Ur, N. Blasi, A. Bracco, F. Camera, S. Leoni, B. Million, M. Pignanelli, G. Pollarolo, A. DeRosa, G. Inglima, M. la Commara, G. la Rana, D. Pierroutsakou, M. Romoli, M. Sandoli, P.G. Bizzeti, A.M. Bizzeti-Sona, G. Lo Bianco, C.M. Petrache, A. Zucchiatti, P. Cocconi, B. Quintana, Ch Beck, D. Curien, G. Duchene, F. Haas, P. Medina, P. Papka, J. Durell, S.J. Freeman, A. Smith, B. Varley, K. Fayz, V. Pucknell, J. Simpson, W. Gelletly, P. Regan, The EUROBALL, PRISMA-2 Collaboration, Coupling a clover detector array with the prisma magnetic spectrometer, Eur. Phys. J. A 20 (1) (2004) 193–197. http://dx.doi.org/10.1140/epja/i2002-10352-9.

[10] J. Simpson, F. Azaiez, G. DeFrance, J. Fouan, J. Gerl, R. Julin, W. Korten, P. Nolan, B. Nyako, G. Sletten, P. Walker, The exogam array: a radioactive beam gamma-ray spectrometer, Acta Physica Hung., Ser. A: Heavy Ion-. Phys. 11 (1–2) (2000) 159–188.

[11] A. Navin, M. Rejmund, C. Schmitt, S. Bhattacharyya, G. Lhersonneau, P.V. Isacker, M. Caamano, E. Clément, O. Delaune, F. Farget, G. de France, B. Jacquot, Towards the high spin-isospin frontier using isotopically-identified fission fragments, Phys. Lett. B 728 (2014) 136–140. http://dx.doi.org/10.1016/j.physletb.2013.11.024.

[12] M. Leino, J. ÅystÃ, T. Enqvist, P. Heikkinen, A. Jokinen, M. Nurmia, A. Ostrowski, W. Trzaska, J. Uusitalo, K. Eskola, P. Armbruster, V. Ninov, Gas-filled recoil separator for studies of heavy elements, Nucl. Instrum. Methods Phys. Res. Sect. B: Beam Interact. Mater. At. 99 (12˘0134) (1995) 653–656. http://dx.doi.org/10.1016/0168-583X(94)00573-7 (application of Accelerators in Research and Industry '94. URL ⟨//www.sciencedirect.com/science/article/pii/0168583×94005737⟩).

[13] C.N. Davids, J.D. Larson, The argonne fragment mass analyzer, Nucl. Instrum. Methods Phys. Res. Sect. B: Beam Interact. Mater. At. 402˘01341 (Part (2)) (1989) 1224–1228. http://dx.doi.org/10.1016/0168-583X(89)90624-1 (URL ⟨//www.sciencedirect.com/science/article/pii/0168583×89906241⟩).

[14] J. Scheurer, M. Aiche, M. Aleonard, G. Barreau, F. Bourgine, D. Boivin, D. Cabaussel, J. Chemin, T. Doan, J. Goudour, M. Harston, A. Brondi, G.L. Rana, R. Moro, E. Vardaci, D. Curien, Improvements in the in-beam g-ray spectroscopy provided by an ancillary detector coupled to a ge g-spectrometer: the diamant-eurogam {II} example, Nucl. Instrum. Methods Phys. Res. Sect. A: Accel., Spectrometers, Detect. Assoc. Equip. 385 (3) (1997) 501–510. http://dx.doi.org/10.1016/S0168-9002(96)01038-8.

[15] O. Skeppstedt, H. Roth, L. Lindstrom, R. Wadsworth, I. Hibbert, N. Kelsall, D. Jenkins, H. Grawe, M. Gorska, M. Moszyski, Z. Sujkowski, D. Wolski, M. Kapusta, M. Hellstrom, S. Kalogeropoulos, D. Oner, A. Johnson, J. Cederkall, W. Klamra, J. Nyberg, M. Weiszflog, J. Kay, R. Griffiths, J.G. Narro, C. Pearson, J. Eberth, The {EUROBALL} neutron wall design and performance tests of neutron detectors, Nucl. Instrum. Methods Phys. Res. Sect. A: Accel., Spectrometers, Detect. Assoc. Equip. 421 (3) (1999) 531–541. http://dx.doi.org/10.1016/S0168-9002(98)01208-X.

[16] B. Cederwall, F.G. Moradi, T. Back, A. Johnson, J. Blomqvist, E. Clément, G. de France, R. Wadsworth, K. Andgren, K. Lagergren, A. Dijon, G. Jaworski, R. Liotta, C. Qi, B.M. Nyakó, J. Nyberg, M. Palacz, H. Al-Azri, A. Algora, G. de Angelis, A. AtaÃ, S. Bhattacharyya, T. Brock, J.R. Brown, P. Davies, A.D. Nitto, Z. Dombrádi, A. Gadea, J. GÃl, B. Hadinia, F. Johnston-Theasby, P. Joshi, K. JuhÃsz, R. Julin, A. Jungclaus, G. Kalinka, S.O. Kara, A. Khaplanov, J. Kownacki, G.L. Rana, S.M. Lenzi, J. Molnár, R. Moro, D.R. Napoli, B.S.N. Singh, A. Persson, F. Recchia, M. Sandzelius, J.-N. Scheurer, G. Sletten, D. Sohler, P.-A. Soderstrom, M.J. Taylor, J.

Timár, J.J. Valiente-Dobón, E.V.. S. Williams, Evidence for a spin-aligned neutron-proton paired phase from the level structure of 92pd, Nature, 469, 2011, pp. 68–71. http://dx.doi.org/10.1038/nature09644.

[17] F. Ghazi Moradi, C. Qi, B. Cederwall, A. Atac, T. Bäck, R. Liotta, M. Doncel, A. Johnson, G. de France, E. Clément, A. Dijon, R. Wadsworth, T.W. Henry, A.J. Nichols, H. Al-Azri, J. Nyberg, A. Gengelbach, T. Hüyük, B.M. Nyakó, J. Timár, D. Sohler, Z. Dombrádi, I. Kuti, K. Juhász, M. Palacz, G. Jaworski, S.M. Lenzi, P.R. John, D.R. Napoli, A. Gottardo, V. Modamio, A. di Nitto, B. Yilmaz, O. Aktas, E. Ideguchi, Character of particle-hole excitations in ^{94}ru deduced from γ-ray angular correlation and linear polarization measurements, Phys. Rev. C 89 (2014) 014301. http://dx.doi.org/10.1103/PhysRevC.89.014301.

[18] F. Ghazi Moradi, B. Cederwall, C. Qi, T. Bäck, A. Atac, R. Liotta, M. Doncel, A. Johnson, G. de France, E. Clément, J. Nyberg, A. Gengelbach, B.M. Nyakó, J. Gál, G. Kalinka, J. Molnár, J. Timár, D. Sohler, Z. Dombrádi, I. Kuti, K. Juhász, D.R. Napoli, A. Gottardo, V. Modamio, R. Wadsworth, T.W. Henry, A.J. Nichols, H. Al-Azri, M. Palacz, E. Ideguchi, O. Aktas, A. di Nitto, A. Dijon, T. Hüyük, G. Jaworski, P.R. John, B. Yilmaz, Spectroscopy of the neutron-deficient $n = 50$ nucleus ^{95}Rh, Phys. Rev. C 89 (2014) 044310. http://dx.doi.org/10.1103/PhysRevC.89.044310.

[19] Y. Zheng, G. de France, E. Clément, A. Dijon, B. Cederwall, R. Wadsworth, T. Bäck, F. Ghazi Moradi, G. Jaworski, B.M. Nyakó, J. Nyberg, M. Palacz, H. Al-Azri, G. de Angelis, A. Atac, O. Aktac, S. Bhattacharyya, T. Brock, P.J. Davies, A. di Nitto, Z. Dombrádi, A. Gadea, J. Gál, P. Joshi, K. Juhász, R. Julin, A. Jungclaus, G. Kalinka, J. Kownacki, G. la Rana, S.M. Lenzi, J. Molnár, R. Moro, D.R. Napoli, B.S. Nara Singh, A. Persson, F. Recchia, M. Sandzelius, J.-N. Scheurer, G. Sletten, D. Sohler, P.-A. Söderström, M.J. Taylor, J. Timár, J.J. Valiente-Dobón, E. Vardaci, γ-ray linear polarization measurements and $(g_{9/2})^{-3}$ neutron alignment in ^{91}ru, Phys. Rev. C 87 (2013) 044328. http://dx.doi.org/10.1103/PhysRevC.87.044328.

[20] K. Andgren, E. Ganioglu, B. Cederwall, R. Wyss, S. Bhattacharyya, J.R. Brown, G.d. Angelis, G.d. France, Z. Dombrádi, J. Gál, B. Hadinia, A. Johnson, F. Johnston-Theasby, A. Jungclaus, A. Khaplanov, J. Kownacki, K. Lagergren, G.L. Rana, J. Molnár, R. Moro, B.S.N. Singh, J. Nyberg, M. Sandzelius, J.-N. Scheurer, G. Sletten, D. Sohler, J. Timár, M. Trotta, J.J. Valiente-Dobón, E. Vardaci, R. Wadsworth, S. Williams, Low-spin collective behavior in the transitional nuclei ^{86,88}Mo, Phys. Rev. C 76 (2007) 014307. http://dx.doi.org/10.1103/PhysRevC.76.014307.

[21] C. Schmitt, M. Rejmund, A. Navin, B. Lecornu, B. Jacquot, G. de France, A. Lemasson, A. Shrivastava, P. Greenlees, J. Uusitalo, K. Subotic, L. Gaudefroy, C. Theisen, B. Sulignano, O. Dorvaux, L. StuttgÃ, New gas-filled mode of the large-acceptance spectrometer {VAMOS}, Nucl. Instrum. Methods Phys. Res. Sect. A: Accel., Spectrometers, Detect. Assoc. Equip. 621 (120133) (2010) 558–565. http://dx.doi.org/10.1016/j.nima.2010.03.146.

[22] C. Theisen, F. Jeanneau, B. Sulignano, F. Druillole, J. Ljungvall, B. Paul, E. Virique, P. Baron, H. Bervas, E. Clément, E. Delagnes, A. Dijon, E. Dossat, A. Drouart, F. Farget, C. Flouzat, G.D. France, A. Goergen, C. Houarner, B. Jacquot, W. Korten, G. Lebertre, B. Lecornu, L. Legeard, A. Lermitage, S. Lhenoret, C. Marry, C. Maugeais, L. Menager, O. Meunier, A. Navin, F. Nizery, A. Obertelli, E. Rauly, B. Raine, M. Rejmund, J. Ropert, F. Saillant, H. Savajols, C. Schmitt, M. Tripon, E. Wanlin, G. Wittwer, Musett: a segmented si array for recoil-decay-tagging studies at {VAMOS}, Nucl. Instrum. Methods Phys. Res. Sect. A: Accel., Spectrometers, Detect. Assoc. Equip. 747 (2014) 69–80. http://dx.doi.org/10.1016/j.nima.2014.02.016.

[23] S. Akkoyun, A. Algora, B. Alikhani, F. Ameil, G. de Angelis, L. Arnold, A. Astier, A. Ataac, Y. Aubert, C. Aufranc, A. Austin, S. Aydin, F. Azaiez, S. Badoer, D. Balabanski, D. Barrientos, G. Baulieu, R. Baumann, D. Bazzacco, F. Beck, T. Beck, P. Bednarczyk, M. Bellato, M. Bentley, G. Benzoni, R. Berthier, L. Berti, R. Beunard, D. Bianco, B. Birkenbach, P. Bizzeti, A. Bizzeti-Sona, F.L. Blanc, J. Blasco, N. Blasi, D. Bloor, C. Boiano, M. Borsato, D. Bortolato, A. Boston, H. Boston, P. Bourgault, P. Boutachkov, A. Bouty, A. Bracco, S. Brambilla, I. Brawn, A. Brondi, S. Broussard, B. Bruyneel, D. Bucurescu, I. Burrows, A. Burger, S. Cabaret, B. Cahan, E. Calore, F. Camera, A. Capsoni, F. Carrio, G. Casati, M. Castoldi, B. Cederwall, J.L. Cercus, V. Chambert, M.E. Chambit, R. Chapman, L. Charles, J. Chavas, E. Clement, P. Cocconi, S. Coelli, P. Coleman-Smith, A. Colombo, S. Colosimo, C. Commeaux, D. Conventi, R. Cooper, A. Corsi, A. Cortesi, L. Costa, F. Crespi, J. Cresswell, D. Cullen, D. Curien, A. Czermak, D. Delbourg, R. Depalo, T. Descombes, P. Desesquelles, P. Detistov, C. Diarra, F. Didierjean, M. Dimmock, Q. Doan, C. Domingo-Pardo, M. Doncel, F. Dorangeville, N. Dosme, Y. Drouen, G. Duchene, B. Dulny, J. Eberth, P. Edelbruck, J. Egea, T. Engert, M. Erduran, S. Erturk, C. Fanin, S. Fantinel, E. Farnea, T. Boutachkov, M. Filliger, F. Filmer, C. Finck, G. de France, A. Gadea, W. Gast, A. Geraci, J. Gerl, R. Gernhauser, A. Giannatiempo, A. Giaz, L. Gibelin, A. Givechev, N. Goel, V. Gonzalez, A. Gottardo, X. Grave, J. Grebosz, R. Griffiths, A. Grint, P. Gros, L. Guevara, M. Gulmini, A. Gorgen, H. Ha, T. Habermann, L. Harkness, H. Harroch, K. Hauschild, C. He, A. Hernandez-Prieto, B. Hervieu, H. Hess, T. Huyuk, E. Ince, R. Isocrate, G. Jaworski, A. Johnson, J. Jolie, P. Jones, B. Jonson, P. Joshi, D. Judson, A. Jungclaus, M. Kaci, N. Karkour, M. Karolak, A. Gorgen, M. Kebbiri, R. Kempley, A. Khaplanov, S. Klupp, M. Kogimtzis, I. Kojouharov, A. Korichi, W. Korten, T. Kroell, R. Krucken, N. Kurz, B. Ky, M. Labiche, X. Lafay, L. Lavergne, M. Lazarus, S. Leboutelier, F. Lefebvre, E. Legay, L. Legeard, F. Lelli, S. Lenzi, S. Leoni, A. Lermitage, D. Lersch, J. Leske, S. Letts, S. Lhenoret, R. Lieder, D. Linget, J. Ljungvall, A. Lopez-Martens, A. Lotode, S. Lunardi, A. Maj, J. van der Marel, Y. Mariette, N. Marginean, R. Marginean, G. Maron, A. Mather, W. Meczynski, V. Mendez, P. Medina, B. Melon, R. Menegazzo, D. Mengoni, E. Merchan, L. Mihailescu, C. Michelagnoli, J. Mierzejewski, L. Milechina, B. Million, K. Mitev, P. Molini, D. Montanari, S. Moon, F. Morbiducci, R. Moro, P. Million, O. Moller, A. Nannini, D. Napoli, L. Nelson, M. Nespolo, V. Ngo, M. Nicoletto, R. Nicolini, Y.L. Noa, B. Nolan, M. Norman, J. Nyberg, A. Obertelli, A. Olariu, R. Orlandi, D. Oxley, C. Ozben, M. Ozille, C. Oziol, E. Pachoud, M. Grave, J. Palin, J. Pancin, C. Parisel, P. Pariset, G. Pascovici, R. Peghin, L. Pellegri, A. Perego, S. Perrier, M. Gibelin, P. Petkov, C. Petrache, E. Pierre, N. Pietralla, S. Pietri, M. Pignanelli, I. Piqueras, Z. Podolyak, P.L. Pouhalec, J. Pouthas, D. Pugnere, V. Pucknell, A. Pullia, B. Quintana, R. Raine, G. Rainovski, L. Ramina, G. Rampazzo, G.L. Rana, M. Rebeschini, F. Recchia, N. Redon, M. Reese, P. Reiter, P. Regan, S. Riboldi, M. Richer, M. Rigato, S. Rigby, G. Ripamonti, A. Robinson, J. Robin, J. Colosimo, J.-A. Ropert, B. Rosse, C.R. Alvarez, D. Rosso, B. Rubio, D. Rudolph, F. Saillant, E. Sahin, F. Salomon, A. Salsac, J. Salt, G. Salvato, J. Sampson, E. Sanchis, C. Santos, H. Schaffner, M. Schlarb, D. Scraggs, O. Seddon, M. Senyigit, M.-H. Sigward, G. Simpson, J. Simpson, M. Slee, J. Smith, P. Sona, B. Sowicki, P. Spolaore, C. Stahl, T. Stanios, E. Stefanova, O. Stezowski, J. Strachan, G. Suliman, P.-A. Soderstrom, J. Tain, S. Tanguy, S. Tashenov, C. Theisen, J. Cederwall, F. Tomasi, N. Toniolo, R. Touzery, B. Travers, A. Triossi, M. Tripon, K. Tun-Lanoe, M. Turcato, C. Unsworth, C. Ur, J. Valiente-Dobón, V. Vandone, E. Vardaci, R. Venturelli, F. Veronese, C. Veyssiere, E. Viscione, R. Wadsworth, P. Walker, N. Warr, C. Weber, D. Weisshaar, D. Wells, O. Wieland, A. Wiens, G. Wittwer, H. Wollersheim, F. Zocca, N. Zamfir, M. Zieblinski, A. Zucchiatti, Agata advanced {GAmma} tracking array, Nucl. Instrum. Methods Phys. Res. Sect. A: Accel., Spectrometers, Detect. Assoc. Equip. 668 (2012) 26–58. http://dx.doi.org/10.1016/j.nima.2011.11.081.

[24] A. Gadea, E. Farnea, J. Valiente-Dobón, B. Million, D. Mengoni, D. Bazzacco, F. Recchia, A. Dewald, T. Pissulla, W. Rother, G. de Angelis, A. Austin, S. Aydin, S. Badoer, M. Bellato, G. Benzoni, L. Berti, R. Beunard, B. Birkenbach, E. Bissiato, N. Blasi, C. Boiano, D. Bortolato, A. Bracco, S. Brambilla, B. Bruyneel, E. Calore, F. Camera, A. Capsoni, J. Chavas, P. Cocconi, S. Coelli, A. Colombo, D. Conventi, L. Costa, L. Corradi, A. Corsi, A. Cortesi, F. Crespi, N. Dosme, J. Eberth, S. Fantinel, C. Fanin, E. Fioretto, C. Fransen, A. Giaz, A. Gottardo, X. Grave, J. Grebosz, R. Griffiths, E. Grodner, M. Gulmini, T. Habermann, C. He, H. Hess, R. Isocrate, J. Jolie, P. Jones, A. Latina, E. Legay, S. Lenzi, S. Leoni, F. Lelli, D. Lersch, S. Lunardi, G. Maron, R. Menegazzo, C. Michelagnoli, P. Molini, G. Montagnoli, D. Montanari, O. Moller, D. Napoli, M. Nicoletto, R. Nicolini, M. Ozille, G. Pascovici, R. Peghin, M. Pignanelli, V. Pucknell, A. Pullia, L. Ramina, G. Rampazzo, M. Rebeschini, P. Reiter, S. Riboldi, M. Rigato, C.R. Alvarez, D. Rosso, G. Salvato, J. Strachan, E. Sahin, F. Scarlassara, J. Simpson, A. Stefanini, O. Stezowski, F. Tomasi, N. Toniolo, A. Triossi, M. Turcato, C. Ur, V. Vandone, R. Venturelli, F. Veronese, C. Veyssiere, E. Viscione, O. Wieland, A. Wiens, F. Zocca, A. Zucchiatti, Conceptual design and infrastructure for the installation of the first {AGATA} sub-array at {LNL}, Nucl. Instrum. Methods Phys. Res. Sect. A: Accel., Spectrometers, Detect. Assoc. Equip. 654 (1) (2011) 88–96. http://dx.doi.org/10.1016/j.nima.2011.06.004.

[25] N., Pietralla, M., Reese, M.L., Cortes, F., Ameil, D., Bazzacco, M.A., Bentley, P., Boutachkov, C., Domingo-Pardo, A., Gadea, J., Gerl, N., Goel, P., Golubev, M., GÃrska, G., Guastalla, T., Habermann, I., Kojouharov, W., Korten, E., MerchÃn, S., Pietri, D., Ralet, P., Reiter, D., Rudolph, H., Schaffner, P.P., Singh, O., Wieland, H. J., Wollersheim, On the road to fair in: Proceedings of the 1st operation of agata in prespec at gsi, EPJ Web of Conferences, 66, 2014, 02083. http://dx.doi.org/10.1051/epjconf/20146602083.

[26] D. Ralet, S. Pietri, Y. Aubert, M. Bellato, D. Bortolato, S. Brambilla, F. Camera, N. Dosme, A. Gadea, J. Gerl, P. Golubev, X. Grave, H. Johansson, N. Karkour, A. Korichi, N. Kurz, X. Lafay, E. Legay, D. Linget, N. Pietralla, D. Rudolph, H. Schaffner, O. Stezowski, B. Travers, O. Wieland, Data-flow coupling and data-acquisition triggers for the prespec-agata campaign at {GSI}, Nucl. Instrum. Methods Phys. Res. Sect. A: Accel., Spectrometers, Detect. Assoc. Equip. 786 (2015) 32–39. http://dx.doi.org/10.1016/j.nima.2015.03.025.

[27] N. Lalović, C. Louchart, C. Michelagnoli, R. Perez-Vidal, D. Ralet, J. Gerl, D. Rudolph, T. Arici, D. Bazzacco, E. Clément, A. Gadea, I. Kojouharov, A. Korichi, M. Labiche, J. Ljungvall, A. Lopez-Martens, J. Nyberg, N. Pietralla, S. Pietri, O. Stezowski, Performance of the {AGATA} g-ray spectrometer in the prespec set-up at {GSI}, Nucl. Instrum. Methods Phys. Res. Sect. A: Accel., Spectrometers, Detect. Assoc. Equip. 806 (2016) 258–266. http://dx.doi.org/10.1016/j.nima.2015.10.032.

[28] A. Maj, et al., The paris project, Acta Physica Pol. B 40 (2009) 565.

[29] J.-M. Régis, G. Pascovici, J. Jolie, M. Rudigier, The mirror symmetric centroid difference method for picosecond lifetime measurements via coincidences using very fast labr3(ce) scintillator detectors, Nucl. Instrum. Methods Phys. Res. Sect. A: Accel., Spectrometers, Detect. Assoc. Equip. 622 (1) (2010) 83–92. http://dx.doi.org/10.1016/j.nima.2010.07.047.

[30] O.J. Roberts, A.M. Bruce, P.H. Regan, Z. PodolyÃk, C.M. Townsley, J.F. Smith, K.F. Mulholland, A. Smith, A labr3: Ce fast-timing array for {DESPEC} at {FAIR}, Nucl. Instrum. Methods Phys. Res. Sect. A: Accel., Spectrometers, Detect. Assoc. Equip. 748 (2014) 91–95. http://dx.doi.org/10.1016/j.nima.2014.02.037 (URL ⟨http://www.sciencedirect.com/science/article/pii/S0168900214002137⟩).

[31] G. Jaworski, M. Palacz, J. Nyberg, G. de Angelis, G. de France, A.D. Nitto, J. Egea, M. Erduran, S. Erturk, E. Farnea, A. Gadea, V. Gonzalez, A. Gottardo, T. Huyuk, J. Kownacki, A. Pipidis, B. Roeder, P.-A. Soderstrom, E. Sanchis, R. Tarnowski, A. Triossi, R. Wadsworth, J.V. Dobón, Monte carlo simulation of a single detector unit for the neutron detector array {NEDA}, Nucl. Instrum. Methods Phys. Res. Sect. A: Accel., Spectrometers, Detect. Assoc. Equip. 673 (2012) 64–72. http://dx.doi.org/10.1016/j.nima.2012.01.017.

[32] T. Hüyük, A. di Nitto, G. Jaworski, A. Gadea, J. Javier Valiente-Dobón, J. Nyberg, M. Palacz, P.-A. Söderström, R. Jose Aliaga-Varea, G. de Angelis, A. Atac, J. Collado, C. Domingo-Pardo, F.J. Egea, N. Erduran, S. Ertürk, G. de France, R. Gadea, V. González, V. Herrero-Bosch, A. Kaşkaş, V. Modamio, M. Moszynski, E. Sanchis, A. Triossi, R. Wadsworth, Conceptual design of the early implementa-

tion of the neutron detector array (neda) with agata, Eur. Phys. J. A 52 (3) (2016) 55. http://dx.doi.org/10.1140/epja/i2016-16055-8.
[33] J.J. Valiente-Dobón, et al., In preparation (2016).
[34] The gaspard project. URL ⟨http://gaspard.in2p3.fr/index.html⟩.
[35] C. Michelagnoli, The performance of AGATA: From the LNL demonstrator to the GANIL setup, in: Proceedings of the 12th International Conference on Nucleus - Nucle 117 in: Proceedings of the 12th International Conference on Nucleus-Nucleus Collisions 2015, EDP Sciences, Catania, Italy, 2015, p. 10004. http://dx.doi.org/10.1051/epjconf/201611710004 URL ⟨http://hal.in2p3.fr/in2p3-01317114⟩.
[36] C. Michelagnoli, et al., To be submitted.
[37] D. Bazzacco, The advanced gamma ray tracking array {AGATA}, Nuclear Physics A, 746, 2004, pp. 248–254, in: Proceedings of the Sixth International Conference on Radioactive Nuclear Beams (RNB6). http://dx.doi.org/10.1016/j.nuclphysa.2004.09.148.
[38] A. Lopez-Martens, K. Hauschild, A. Korichi, J. Roccaz, J.-P. Thibaud, Ray tracking algorithms: a comparison, Nucl. Instrum. Methods Phys. Res. Sect. A: Accel., Spectrometers Detect. Assoc. Equip. 533 (3) (2004) 454–466. http://dx.doi.org/10.1016/j.nima.2004.06.154.
[39] A. Pullia, D. Barrientos, D. Bazzacco, M. Bellato, D. Bortolato, R. Isocrate, A 12-channel 14/16-bit 100/125-ms/s digitizer with 24-gb/s optical output for agata/galileo, in: 2012 IEEE Nuclear Science Symposium and Medical Imaging Conference Record (NSS/MIC), 2012, pp. 819–823. http://dx.doi.org/10.1109/NSSMIC.2012.6551218.
[40] D. Barrientos, M. Bellato, D. Bazzacco, D. Bortolato, P. Cocconi, A. Gadea, V. GonzÃÂlez, M. Gulmini, R. Isocrate, D. Mengoni, A. Pullia, F. Recchia, D. Rosso, E. Sanchis, N. Toniolo, C.A. Ur, J.J. Valiente-Dobón, Performance of the fully digital fpga-based front-end electronics for the galileo array, IEEE Trans. Nucl. Sci. 62 (6) (2015) 3134–3139. http://dx.doi.org/10.1109/TNS.2015.2480243.
[41] Ceph: The future of storage. URL ⟨http://ceph.com/⟩.
[42] X. Grave, R. Canedo, J. F. Clavelin, S. Du, E. Legay, Narval a modular distributed data acquisition system with ada 95 and rtai, in: Proceedings of the 14th IEEE-NPSS Real Time Conference, 2005, pp. 5. http://dx.doi.org/10.1109/RTC.2005.1547454.
[43] E. Farnea, F. Recchia, D. Bazzacco, T. Kroell, Z. Podolyak, B. Quintana, A. Gadea, Conceptual design and monte carlo simulations of the {AGATA} array, Nucl. Instrum. Methods Phys. Res. Sect. A: Accel., Spectrometers Detect. Assoc. Equip. 621 (120133) (2010) 331–343. http://dx.doi.org/10.1016/j.nima.2010.04.043.
[44] M. Vandebrouck, A. Lemasson, M. Rejmund, G. Fremont, J. Pancin, A. Navin, C. Michelagnoli, J. Goupil, C. Spitaels, B. Jacquot, Dual position sensitive {MWPC} for tracking reaction products at vamos++, Nucl. Instrum. Methods Phys. Res. Sect. A: Accel., Spectrometers, Detect. Assoc. Equip. 812 (2016) 112–117. http://dx.doi.org/10.1016/j.nima.2015.12.040.
[45] A. Dewald, O. Moller, P. Petkov, Developing the recoil distance doppler-shift technique towards a versatile tool for lifetime measurements of excited nuclear states, Prog. Part. Nucl. Phys. 67 (3) (2012) 786–839. http://dx.doi.org/10.1016/j.ppnp.2012.03.003.
[46] J. Ljungvall, G. Georgiev, S. Cabaret, N. Karkour, D. Linget, G. Sedes, R. Chevrier, I. Matea, M. Niikura, M.-D. Salsac, B. Sulignano, The orsay universal plunger system, Nucl. Instrum. Methods Phys. Res. Sect. A: Accel., Spectrometers, Detect. Assoc. Equip. 679 (2012) 61–66. http://dx.doi.org/10.1016/j.nima.2012.03.041.
[47] Muscade us.c.a.d.a for embedded system and pc. URL ⟨http://www.irfu.cea.fr/Sis/products/www/muscade/⟩.
[48] M. Bellato, D. Bortolato, J. Chavas, R. Isocrate, G. Rampazzo, A. Triossi, D. Bazzacco, D. Mengoni, F. Recchia, Sub-nanosecond clock synchronization and trigger management in the nuclear physics experiment agata, J. Instrum. 8 (07) (2013) P07003.
[49] Mfm - multiframe metaformat. URL ⟨http://www.informatique.in2p3.fr/?Q=mfm⟩.
[50] G. Wittwer, F. Saillant, M. Blaizot, G.F. Grinyer, B. Raine, C. Belkhiria, S. Primault, C. Gueye, Microtca.0, a shelf standard adopted by the get project for experiments in nuclear physics with the smart trigger and time stamper mutant, in: 2014 Proceedings of the 19th IEEE-NPSS Real Time Conference, 2014, pp. 1–5.
[51] R. Brun, F. Rademakers, {ROOT}: An object oriented data analysis framework, Nucl. Instrum. Methods Phys. Res. Sect. A: Accel., Spectrometers Detect. Assoc. Equip. 389 (120132) (1997) 81–86. http://dx.doi.org/10.1016/S0168-9002(97)00048-X (new Computing Techniques in Physics Research V).
[52] Agata data analysis. URL ⟨http://agata.in2p3.fr/⟩.
[53] S. Agostinelli, J. Allison, K. Amako, J. Apostolakis, H. Araujo, P. Arce, M. Asai, D. Axen, S. Banerjee, G. Barrand, F. Behner, L. Bellagamba, J. Boudreau, L. Broglia, A. Brunengo, H. Burkhardt, S. Chauvie, J. Chuma, R. Chytracek, G. Cooperman, G. Cosmo, P. Degtyarenko, A. Dellacqua, G. Depaola, D. Dietrich, R. Enami, A. Feliciello, C. Ferguson, H. Fesefeldt, G. Folger, F. Foppiano, A. Forti, S. Garelli, S. Giani, R. Giannitrapani, D. Gibin, J.G. Cadenas, I. GonzÃÂlez, G.G. Abril, G. Greeniaus, W. Greiner, V. Grichine, A. Grossheim, S. Guatelli, P. Gumplinger, R. Hamatsu, K. Hashimoto, H. Hasui, A. Heikkinen, A. Howard, V. Ivanchenko, A. Johnson, F. Jones, J. Kallenbach, N. Kanaya, M. Kawabata, Y. Kawabata, M. Kawaguti, S. Kelner, P. Kent, A. Kimura, T. Kodama, R. Kokoulin, M. Kossov, H. Kurashige, E. Lamanna, T. LampÃÂn, V. Lara, V. Lefebure, F. Lei, M. Liendl, W. Lockman, F. Longo, S. Magni, M. Maire, E. Medernach, K. Minamimoto, P.M. de Freitas, Y. Morita, K. Murakami, M. Nagamatu, R. Nartallo, P. Nieminen, T. Nishimura, K. Ohtsubo, M. Okamura, S. Oneale, Y. Oohata, K. Paech, J. Perl, A. Pfeiffer, M. Pia, F. Ranjard, A. Rybin, S. Sadilov, E.D. Salvo, G. Santin, T. Sasaki, N. Savvas, Y. Sawada, S. Scherer, S. Sei, V. Sirotenko, D. Smith, N. Starkov, H. Stoecker, J. Sulkimo, M. Takahata, S. Tanaka, E. Tcherniaev, E.S. Tehrani, M. Tropeano, P. Truscott, H. Uno, L. Urban, P. Urban, M. Verderi, A. Walkden, W. Wander, H. Weber, J. Wellisch, T. Wenaus, D. Williams, D. Wright, T. Yamada, H. Yoshida, D. Zschiesche, Geant4 simulation toolkit, Nucl. Instrum. Methods Phys. Res. Sect. A: Accel., Spectrometers, Detect. Assoc. Equip. 506 (3) (2003) 250–303. http://dx.doi.org/10.1016/S0168-9002(03)01368-8.